Coincidences between Gravitational Wave Interferometers and High Energy Neutrino Telescopes

Thierry PRADIER
Institut Pluridisciplinaire Hubert Curien (IPHC/DRS)
&
University Louis-Pasteur, Strasbourg (France)

Abstract

Sources of gravitational waves (GW) and emitters of high energy (HE) neutrinos both involve compact objects and matter moving at relativistic speeds. GW emission requires a departure from spherical symmetry, which is the case if clumps of matter are accreted around black holes or neutron stars, and ejected in relativistic jets, where neutrinos are believed to be produced. Both messengers interact weakly with the surrounding matter, hence point directly to the heart of the engines that power these emissions. Coincidences between GW interferometers (*e.g.* VIRGO) and HE ν telescopes (*e.g.* ANTARES) would then give a unique insight on the physics of the most powerful objects in the Universe. The possibility, observability and detectability for such GW/HE ν coincidences are analysed.

Key words: Neutrino telescopes, gravitational wave interferometers, X-ray binaries, soft gamma repeaters
PACS: 95.55.Vj, 95.85.Ry, 95.55.Ym, 95.85.Sz

1. Scientific motivations

The forthcoming years should be very exciting both in gravitational wave (GW) astronomy and high energy neutrino (HE ν) astronomy. The VIRGO interferometer [1], currently closed down for upgrade, should be taking data with an improved injection system in 2009, whereas the ANTARES collaboration has completed the deployment and connections of its 12 lines [2] early in June 2008, starting the operation of the first *undersea* neutrino telescope. In the mean time, the two LIGO interferometers (ITF) are in operation [3], and ICECUBE is deploying its 1 km^3 neutrino telescope in the ice of the South Pole, already having 40 lines in data taking mode [4].

Both GW sources and HE ν emitters involve compact objects and matter moving at relativistic speeds. As a result, coincidences between GW interferometers and neutrino telescopes can be envisaged [5], and should then be feasible by 2009, with the joint operation of VIRGO, LIGO, ANTARES and ICECUBE. Together, they would give a unique insight on the physics of the most powerful objects in the Universe. Some classes of astrophysical object, invisible in electromagnetic channels, may be observable only *via* their gravitational waves and high energy neutrino emissions. Finally, in many quantum gravity (QG) models [6], the propagation velocity of a particle depends on the energy:

$$c^2p^2 = E^2\left[1 + \xi\left(\frac{E}{E_{\rm QG}}\right) + \mathcal{O}\left(\frac{E^2}{E_{\rm QG}^2}\right) + \ldots\right] \quad (1)$$

where $|\xi| \simeq 1$, and $E_{\rm QG}$ is the energy scale at which QG effects arise. Hence, measuring a non-zero time delay between gravitational wave bursts and high energy neutrino transients would then allow to probe Quantum Gravity effects at the Planck energy level.

Such time coincidences require GW bursts (localized in time), and would allow GW antennae to confirm a burst detection, and neutrino telescopes to sign the cosmic origin of the signal. It must be first demonstrated that such a coincidence process is:

- possible: sources of both GW and HE ν, able to emit signals possibly coincident in time, exist in the Galaxy. This is discussed in section 2;
- observable: the visibility sky maps of VIRGO and ANTARES are not orthogonal. This point is addressed in section 3 ;
- detectable: the resulting coincidence detection probability, for a fixed accidental coincidence rate, which constrains the authorized background level for each individual detector, must be estimated. This point is developed in section 4.

2. GW bursters and HE ν sources

Only *galactic* potential sources of both GW and HE ν signals will be discussed here, for two reasons. Firstly, the only sources accessible with first generations detectors such as ANTARES and VIRGO are likely to be galactic ones. Secondly, for sources in the local universe, in particular with negligible redshift, the QG delay mentionned in the previous section is independent of cosmological models. This (non-exhaustive) section focuses on microquasars and soft-gamma repeaters, however core-collapse supernovae and gamma-ray bursts are commonly cited extra-galactic sources of both GW and ν emissions: these are described elsewhere [7].

2.1. *Outbursts from microquasars*

Microquasars are galactic jet sources associated with some classes of X-ray binaries involving both neutron stars and black hole candidates. During active states, the X-ray flux and spectrum can vary substantially, with a total luminosity that, during the so-called very high states, often exceeds the Eddington limit [8]. Their activity involves ejection within jets with kinetic power that appears to constitute a considerable fraction of the liberated accretion energy, giving rise to intense radio and IR flares. Radio monitoring of some X-ray transients has revealed superluminal motions in some objects, indicating that the jets are relativistic, with $\gamma \sim 1-10$. The ejection episodes are classified into several classes according to the brightness of synchrotron emission produced in the jet and the characteristic time scale of the event. The duration of major ejection events is typically on the order of days, while that of less powerful flares is correspondingly shorter (minutes to hours). The correlations between the X-ray and synchrotron emission clearly indicates a connection between the accretion process and the jet activity. Whether radio and IR outbursts represent actual ejection of blobs of plasma or, alternatively, formation of internal shocks in a quasi-steady jet is unclear. In any case, since the overall time scale of outbursts is much longer than the dynamical time of the compact object (milliseconds), it is likely that shocks will continuously form during the ejection event. If a fraction of at least a few percent of the jet power is used to accelerate electrons to very high energies then emission of high-energy gamma rays is anticipated, in addition to the observed radio and IR emission.

2.1.1. *High energy neutrino emission*

The content of jets in microquasars remains an open issue. In scenarios in which an initial rise of the X-ray flux leads an ejection of the inner part of the accretion disk, as is widely claimed to be suggested by the anticorrelation between the X-ray and radio flares seen during major ejection events, e-p jets are expected to be produced. A possible diagnostic of e-p jets is the presence of Doppler-shifted spectral lines, such as the Hα line as seen in SS433.

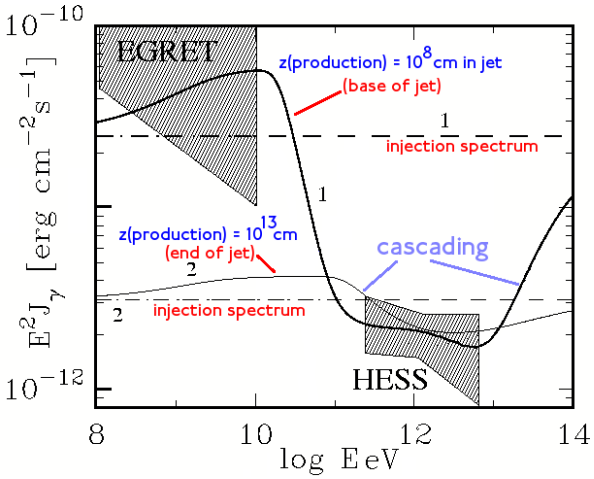

Fig. 1. γ Data from EGRET and HESS, together with predictions for models with production of γ at the base or at the end of the jet.

Taking the example of LS 5039, some authors argue in favor of hadronic origin of TeV photons [9], especially if they are produced within the binary

system. The detected γ-rays should be accompanied by a flux of high energy neutrinos emerging from the decays of $\pi^{\pm}$ mesons produced at pp and/or pγ interactions. The flux of TeV neutrinos, which can be estimated on the basis of the detected TeV γ-ray flux, taking into account the internal $\gamma\gamma \rightarrow e^+e^-$ absorption, depends significantly on the location of γ-ray production region. The minimum neutrino flux above 1 TeV is expected to be at the level of 10^{12} cm^{2}s^{-1}, but could be up to a factor of 100 higher. As can be seen in figure 1 (taken from [9]), the HESS/EGRET data agree well with a production of γ (and neutrinos) at the base of the jet, very close to the onset of the acceleration phase and its corresponding GW signal (see section 2.1.2). Finally, one should note that the detectability by ANTARES or future km^3 telescopes depends strongly on the high energy cutoff in the spectrum of parent protons.

2.1.2. *GW emission during a powerful flaring event*

Two kinds of processes could lead to detectable GW signals [10]. Firstly, the matter accreted for months/years could be *swallowed* by the compact object, and, provided that the process is fast, trigger the resonance of normal modes in the central object. Secondly, the acceleration of the matter in the jet is the origin of a short GW burst.

For both signals, the amplitude will depend critically on the accreted/ejected mass. The assumption which is made in the following is that all the matter ejected during a flare comes from the accretion disk, and had previously fallen onto the compact object at some previous moment. The GW emission produced by the infall of matter onto the central object is different in the case of neutron stars (NS) and black holes (BH), but in both cases results in the excitation of the Quasi-Normal Modes of the star [11] (typically a damped sine signal) which could continue into the ejection phase. The time-lag between the two processes is unknown, and could range from ms up to several days.

In the NS case, the characteristic amplitude (scaling as $1/d$) at 1 kpc can be written as $h_c \approx 10^{-20} \left(\frac{\eta}{10^{-6}}\right)^{1/2} f_0^{-\frac{1}{2}}$ for the accretion signal [11], to be compared with the VIRGO sensitivity $h_{\rm noise} \sim 10^{-21}$ around 1 kHz. $\delta m = \eta \mathrm{M}_\odot$ is the accreted/ejected mass, and f_0 the frequency of the excitation. Note that this assumes a sudden infall of the matter onto the compact object (*bursting mode*), and does not stand if the accretion infall is a continuous and slow process (*continuous mode*).

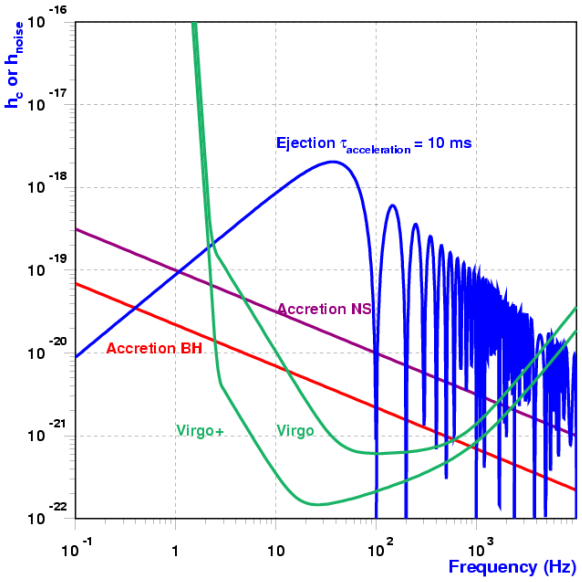

Fig. 2. Amplitudes expected for the accretion/ejection processes at 1 kpc, for $\delta m \sim 10^{-4}\mathrm{M}_\odot$, $\tau_{\rm acc} \sim 10$ ms, $\gamma = 10$.

The acceleration of an ultrarelativistic blob of matter with a Lorentz factor γ around a compact object induces a *burst with memory*, the space-time perturbation reaching a maximum amplitude at 1 kpc $\Delta h \sim 2 \times 10^{-22} \left(\frac{\gamma}{10}\right) \left(\frac{\eta}{10^{-6}}\right)$, independent on the density of the ejecta [12]. The frequency is typically the inverse of the acceleration time $t_{\rm acc}$, ranging from $\Delta t_{\text{free-fall}} \sim 0.1$ ms for a 10 $\mathrm{M}_\odot$ object, up to $\Delta\tau_{\rm max} \sim 1$ min, observations of galactic X-Ray binaries showing that radio emission occurs at a distance ~ 0.1 AU from the central object. A summary of those estimates are displayed in figure 2, for a source at 1 kpc, ejected mass $\delta m \sim 10^{-4}$ $\mathrm{M}_\odot$ and acceleration time $\tau_{\rm acc} \sim 10$ ms.

Taking into account accretion rates (typically $\dot{M} \sim 10^{-8} M_\odot$/yr), jet luminosities ($10^{29}$J/s – 10^{33}J/s) and radio blob sizes $\sim 10^{12}$ m and densities (from 10^{-10}g.cm^{-3} up to 10^{15}g.cm^{-3}), the accreted/ejected mass for major events can be estimated to range from $10^{-8}\mathrm{M}_\odot$ up to $10^{-4}\mathrm{M}_\odot$, with an average mass of $10^{-6}\mathrm{M}_\odot$. Thus the amplitudes shown in figure 2 correspond to the maximum mass and Lorentz factor that can be expected. Nonetheless, such extreme outbursts, where the matter accreted over months or even years, is swallowed and then ejected in one single bursting event cannot be ruled out.

2.2. *Flares from Soft-Gamma Repeaters*

Soft gamma-ray repeaters (SGRs) are X-ray pulsars which have quiescent soft (2-10 keV) periodic X-ray emissions with periods ranging from 5 to 10 s. They exhibit repetitive bursts lasting ~ 0.1 s which reach peak luminosities of $\sim 10^{34}$ J/s, in X-rays and γ-rays. There are 4 known SGRs, 3 in the Milky Way, and one in the Large Magellanic Cloud. Three of the 4 have had hard spectrum (MeV energy) giant flares with luminosities up to 10^{40} J/s. The favoured *magnetar* model for these objects is a neutron star with a huge magnetic flied $B \sim 10^{15}$ G [13]. Star-quakes are thought to fracture the rigid crust causing outbursts. These giant flares result from the formation and dissipation of strong localized currents coming from magnetic field rearrangements associated with the quakes, liberating a high flux of X- and γ-rays.

Sudden changes in the large magnetic fields would accelerate protons or nuclei that produce neutral and charged pions in interactions with thermal radiation. These subsequently decay into TeV or even PeV energies γ-rays and neutrinos [14]. Flares from SGRs are thus potential sources of high energy neutrinos.

During the crustal disruption, a fraction of the initial magnetic energy is annihilated and released as photons, and the stored elastic energy is also converted into shear vibrations with frequencies in the kHz regime. These waves are able to excite non-radial modes, damped by GW emission [15]. The expected gravitational strain amplitude can be written as:

$$h(t) = \frac{2}{d\omega_n}\left(\frac{GE}{c^3\tau_n}\right)^{\frac{1}{2}} e^{\left(i\omega_n t - \frac{t}{\tau_n}\right)}, \qquad (2)$$

where E is the total energy, G the gravitational constant, ω_n and τ_n the pulsation and damping timesale of the n-mode. These oscillation parameters depends on the equation of state and the stellar mass. Simulations [15] show that low mass stars produce larger gravitational amplitudes and could be detected more deeply within the Galaxy. Moreover, sources at distances ranging from 0.4 kpc up to 2.4 kpc could be probed with the planned sensitivity of Virgo. The detection probability and frequency of these events depend on the poorly constrained distribution of this class of sources in the Galaxy.

3. Observability of Coincidences

Both GW detectors and HE ν telescopes have limited sky coverage and exposure. In order to perform coincidences between both types of detector, the overlap of such visibility maps has to be computed: the following paragraphs address this question, taking the examples of Virgo and Antares.

3.1. Virgo *beam pattern*

The response $h(t)$ of an interferometric detector to a GW is a linear combination of the two independent wave polarizations h_+ and $h_\times$, with weighting factors called the beam pattern functions: they have values in the range $[-1;1]$, depending on the longitude and latitude of the detector location, as well as its orientation, the angle between the arms, the sky coordinates of the source, and the wave polarization angle. The best response is achieved for detectors with orthogonal arms. In the following, average over the unknown polarization angle will be presented. The instantaneous beam pattern (normalised to its maximal value) at a given time during the day, in equatorial coordinates (right ascension α, declination δ), is displayed in figure 3 for Virgo.

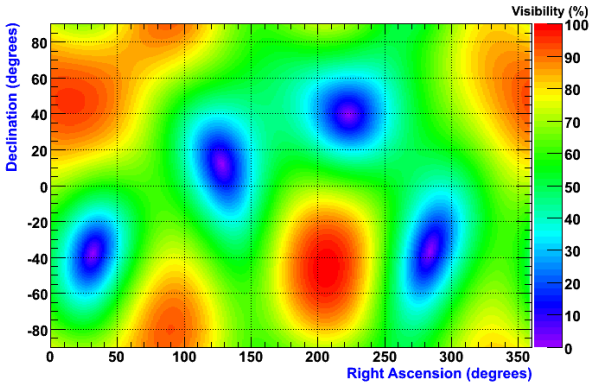

Fig. 3. Virgo beam pattern in equatorial coordinates.

3.2. Antares *visible sky*

Antares is only sensitive to sources below the horizon at some time during the day, because it searches for neutrinos which have interacted in the Earth: a portion of the sky is therefore never visible. Figure 4 shows the daily average visibility as a function of $\sin\delta$.

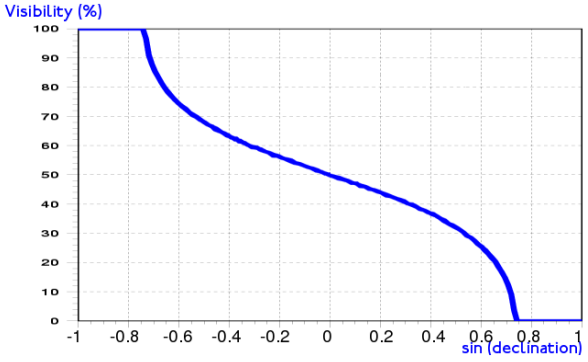

Fig. 4. ANTARES daily averaged visibility *vs* $\sin\delta$.

3.3. ANTARES/VIRGO *common sky*

The visibility sky map for coincidences between ANTARES and VIRGO is the convolution of the two previous exposure maps. The daily averaged common sky map is displayed in figure 5, together with the position of known microquasars and soft-gamma repeaters (or magnetars). Except for three of them, all are visible at some time by both experiments, rendering observable GW/HE ν coincidences for most of these galactic sources.

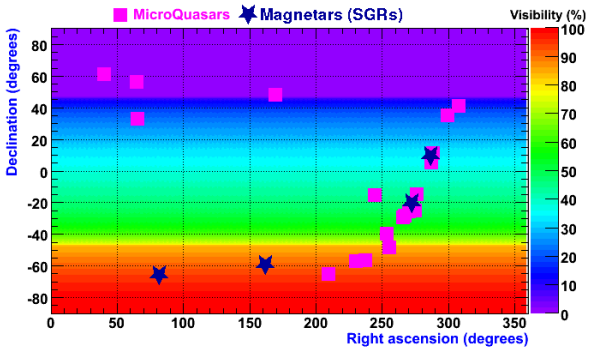

Fig. 5. Common visibility sky map for ANTARES and VIRGO.

4. Detectability of Coincidences

Given GW/HE ν coincidences are observable, at least for the ANTARES and VIRGO couple, the detectability, in terms of detection probability *vs* false alarms rate, has to be evaluated.

4.1. *Coincidence window and QG effects*

To set the coincidence time window, possible physical propagation delays have to be estimated. In the case of GW, the graviton being massless, and the energy carried away by each individual graviton in a GW burst being small ($E_{\rm graviton} \sim hf \ll 1$ for $f = 1$ kHz), QG-induced or mass-induced delays are close to zero. For a 1 TeV ν, the mass-induced delay is negligible even with $m_\nu = 1$ eV. Taking the expression given in eq. 1 as a starting point, with $\xi = -1$ being favoured, and neglecting any cosmological effects (for low redshift $z \ll 1$), the delay in ms becomes, in the first order:

$$\Delta t^{\rm ms}_{\rm QG} \simeq 0.15 \left(\frac{d}{10\ {\rm kpc}}\right)\left(\frac{E_\nu}{1\ {\rm TeV}}\right)\left(\frac{10^{19}\ {\rm GeV}}{E_{\rm QG}}\right) \quad (3)$$

Taking $E_{\rm QG} = E_{\rm Planck} \sim 10^{19}$ GeV, this yields a maximum QG delay of 1 second for $E_\nu = 1$ PeV and sources up to the Large Magellanic Cloud ($d \sim 50$ kpc), or lower energy neutrinos ($E_\nu \approx 1$ TeV) and sources as far as the Virgo Cluster ($d \sim 20$ Mpc). $\Delta t_{\rm coinc} = 1$ s thus seems a reasonnable choice. Nevertheless, the coincidence time window can also be set by imposing an overall coincidence detection probability for a given GW signal. Detection issues, both for GW ITFs and HE ν telescopes must now be addressed.

4.2. VIRGO *detection*

The detection of a transient signal in a GW ITF is not an easy task. Generally, an allowed false alarm rate is fixed, and the detection probability can be estimated as a function of the signal-to-noise ratio (SNR or ρ) of a particular signal: this is shown for VIRGO in figure 6, for $\rho_{\rm max} = 5$ (defined as the SNR obtained with optimal detector orientation and perfect detection by Wiener filtering), a very low signal, for detection algorithms designed for burst signals [16]. In the best case, a threshold corresponding to 1 false alarm every 5 minutes is needed to obtain a 50% detection probability, without taking into account any beam pattern effects.

The right part of figure 6 displays the detection efficiency as a function of $\rho_{\rm max}$, for this particular false alarm rate, in the case of a single ITF detection or coincident detection in the VIRGO/LIGO network: for low SNRs, the detection by a single ITF is more probable than any twofold coincidence, and the detection by any single ITF is always more efficient than any coincidence configuration [17]. In the case of the detection by any of the 3 ITFs, the directional information is not available (no triangula-

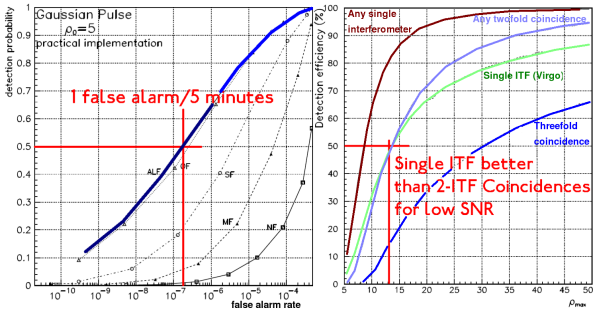

Fig. 6. Left : detection probability *vs* false alarm rate, for a $\rho = 5$ gaussian pulse. Right : detection probability *vs* $\rho_{\max}$ for the different possible detection configurations.

tion), and the only relevant information is therefore the *time* of the burst event.

VIRGO has a sampling frequency of 20 kHZ, and for a gaussian burst of width τ and SNR ρ, the rms error on the burst arrival time is [17]:

$$\Delta t^{\mathrm{RMS}} \approx \frac{1.5}{\mathrm{SNR}} \left(\frac{\tau}{1\ \mathrm{ms}}\right)\ \mathrm{ms}, \qquad (4)$$

yielding a timing resolution below the ms for $\rho > 5$ and short burst. This of course limits the accessible QG energy scale, and the coincidence window to be used.

4.3. ANTARES *detection*

In a neutrino Telescope, the Čerenkov light emitted by the neutrino-induced muon is detected by an array of photomultipliers arranged in strings, able to reconstruct the energy and direction of the incident muon/neutrino. The measurements of the time of the hits and the amplitude of the hits, together with the position of the hits are needed to achieve the reconstruction of the muon track with the desired resolution (below 0.3° above 10 TeV). The quality of the track fit is often expressed in terms of a log-likelihood ratio term $\Lambda \approx \frac{\log(\mathcal{L})}{N_{\mathrm{dof}}}$, the distribution of which is shown in figure 7, for (upward) atmospheric neutrinos and misreconstructed atmospheric muons, together with the signal detection efficiency (*i.e.* the ability to detect within 1° of the true direction a signal neutrino, assuming a E^{-2} spectrum). The standard cut applied is $\Lambda = -5.3$, for which the signal efficiency is close to 75%; the misreconstruted atmospheric muons are decreased to 1/day, and the atmospheric neutrinos to 10/day [18].

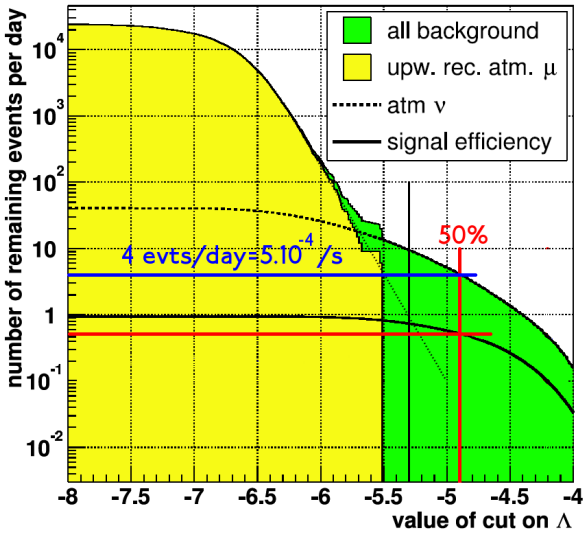

Fig. 7. Number of background events left as a function of the cut value for Λ. The efficiency for signal is also shown.

4.4. *Accidentals and efficiency*

Figures 6 and 7 provide the information needed to estimate the detection probability $\epsilon_{V,A}$ for a background/false alarm level $R_{V,A}$ in both detectors (V for VIRGO, A for ANTARES). The coincidence detection probability is $\epsilon_{\mathrm{coinc}} = \epsilon_V \epsilon_A$, whereas the coincident accidentals rate in a given time window is $R_{\mathrm{coinc}} = R_V R_A \Delta t_{\mathrm{coinc}}$. Setting $\Delta t_{\mathrm{coinc}} = 1$ s and $R_{\mathrm{coinc}} \sim 1/\mathrm{yr}$, the resulting coincidence detection probability is shown in figure 8 as a function of the Λ cut: the efficiency is maximum for $\Lambda \sim -5.5$, below which R_A is too high, resulting in a too high VIRGO detection threshold (for a preset $R_V R_A$).

Equivalently, the coincidence detection probability can be set at *e.g.* 50% for a given signal, and the maximal allowed coincidence time window can be extracted: this is displayed in figure 9, as a function of ANTARES/VIRGO detection probabilities, for a $\rho = 5$ gaussian burst, with $R_{\mathrm{coinc}} \sim 1/\mathrm{yr}$. The time coincidence window is maximal for $\epsilon_V \sim 65\%$, reaching ~ 15 ms.

For such a low accidental rate (1/yr), several coincident detections would be needed to have a high significance, but this nonetheless proves the detectability of GW/HE ν coincidences.

5. ANTARES/VIRGO Coincidences

If a coincidence is indeed observed, the significance of this positive detection can be estimated,

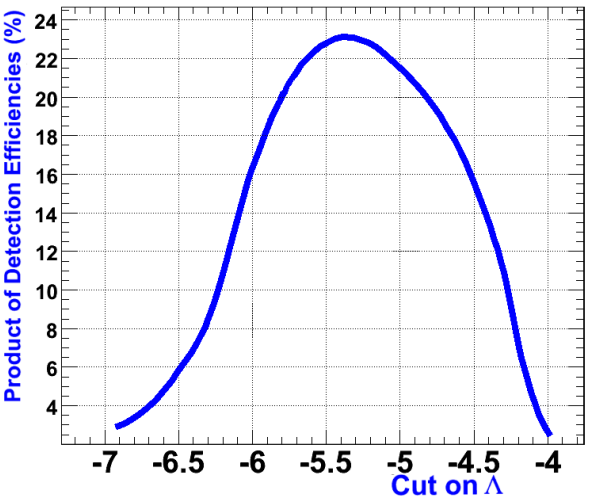

Fig. 8. Coincidence detection probability *vs* Λ cut.

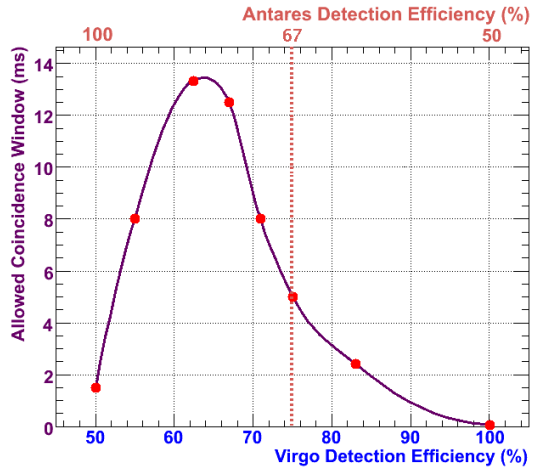

Fig. 9. Maximal allowed coincidence time window in ms vs ANTARES/VIRGO detection probabilities, requiring $\epsilon_{\rm coinc} = 50\%$.

and assuming that both the GW and HE ν signals have been emitted with zero delay at the source, limits can be put on the QG energy scale $E_{\rm QG}$. In the case described in the previous section (requiring $\epsilon_{\rm coinc} = 50\%$), the minimum accessible $E_{\rm QG}$ can be estimated using eq. 1. The maximum energy scale yielding a measurable effect is limited by GW timing resolution, which depends on the burst duration and SNR, and reaches in this case $E_{\rm QG}^{\rm max} \sim 5 \times 10^{18}$ GeV ($\rho = 5$), close to the Planck limit. The minimum accessible energy scale is in turn determined by the maximal coincidence window defined previously, which yields $E_{\rm QG}^{\rm min} \sim 10^{17}$ GeV. This is to be compared with existing limits on $E_{\rm QG}$, *e.g.* using TeV flares from Mrk421 $\sim 4 \times 10^{17}$ GeV [19].

It should be noted that to perform a real *measurement* of $E_{\rm QG}$, the neutrino energy resolution is of importance, and is a factor 2 or 3 in the case of ANTARES [18].

5.1. *Making coincidences*

The process for performing time coincidences is quite classical. VIRGO and ANTARES produce trigger lists, according to some predefined false alarm rates, corresponding to different coincidence time windows. Timeshifts performed on these data streams allow for the study of background coincident triggers; in the *zero-lag* case, ANTARES/VIRGO triggers are compared in predefined time windows. The significance of an observed coincidence is then statistically evaluated by comparing the two cases.

5.2. ANTARES/VIRGO *common calendar*

VIRGO took data jointly with the 2 LIGO interferometers between May and September 2007, during the *Virgo Scientific Run* (VSR), achieving the sensitivity shown in figure 10, together with the sensitivities obtained during previous commissioning or science runs (weekly runs from september 2006 until march 2007). In spite of problems with the laser injection system (at low frequency), and a factor 2 difference at high frequency, the resulting sensitivity is quite close to the expectation. The interferometer should be taking data again with an improved injection system in 2009.

ANTARES has been taking data continuously with its final 12 line configuration since the end of May 2008, and is expected to observe high energy neutrinos for a period of 10 years. Interestingly, during the *VSR*, ANTARES already had 5 lines operational since January 2007. Clearly, during this parallel operation of VIRGO and ANTARES 5-lines, only the most powerful GW/HE ν sources could be detected; however these data could be used as a *test bench* for preliminary studies on time coincidences. Moreover, LIGO data, which are also available for this *VSR*/5-lines period, could be used to enhance the detection probability, a detection by any of the 3 interferometers being more efficient than for VIRGO alone (see section 4).

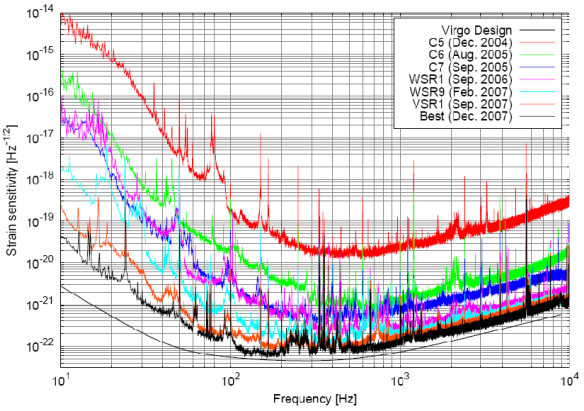

Fig. 10. VIRGO sensitivity curves from Commissioning Runs to Science Runs.

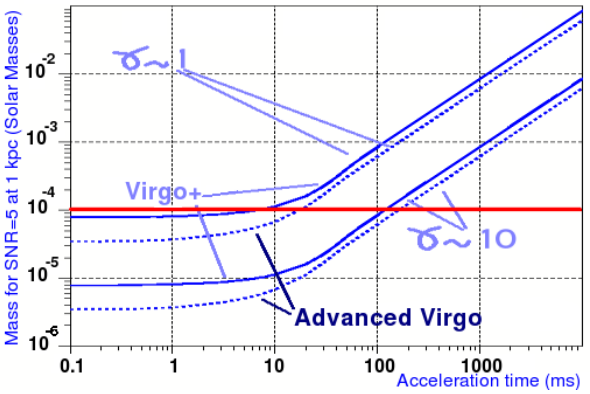

Fig. 11. Ejected mass needed for SNR=5 for a microquasar at 1 kpc for VIRGO+ and ADVANCED VIRGO.

Aknowledgements : *I would like to thank the Organizing Committee, especially John Carr, for trusting me for this plenary talk.*

6. Conclusions

Time coincidences between GW interferometers, such as VIRGO, currently down for upgrade, and high energy neutrino telescopes, such as ANTARES, now fully operational, are thus feasible: common sources able to emit coincident signals in both channels exist in our own galaxy. Microquasars, during major outbursts, and flares from SGRs are possible targets. ANTARES and VIRGO visibility sky maps are not othogonal, allowing for coincident detections. Taking into account the relationship between detection efficiencies and false alarm rates in ANTARES and VIRGO, coincident observations appear possible.

Such coincidences can be performed using ANTARES 5-lines and *VSR* data (end of 2007) as a test that could be performed before the upgrade of VIRGO next year, which should improve the sensitivity at low and high frequency to reach the design sensitivity. This VIRGO+ upgrade will correspond with the *routine* operation of the full ANTARES detector, provinding the opportunity to perform the time coincidences presented in this paper.

Finally, *circa* 2015, a km^3 neutrino telescope should be operating in the Mediterranean Sea [20], along with an ADVANCED VIRGO interferometer [21], with enhanced sensitity at low frequency. Figure 11 [10] shows the ejected mass needed in a microquasar ejection event to obtain a SNR = 5 in VIRGO+ and ADVANCED VIRGO [21] as a function of the acceleration time (see section 2): less extremes ejection scenarios could be probed, and interesting constraints on accretion/ejection models could be set by this novel multimessenger approach.

References

[1] VIRGO Collaboration, Nucl. Phys. Proc. Suppl. **54B** 167-175 (1997); see also : VIRGO, *AIPC* **924**, 187-193 (2007)
[2] M. Circella, for ANTARES, these proceedings
[3] LIGO Collaboration, Classical & Quantum Gravity **25** 114041 (2008)
[4] E. Resconi, for ICECUBE, these proceedings
[5] Y. Aso *et al.*, Classical & Quantum Gravity **25** 114039 (2008)
[6] S. Choubey & S. F. King, Phys. Rev. **D67** 073005 (2003)
[7] *e.g.* GRB GWs: M. H. van Putten *et al.*, Phys. Rev. **D69** 044007 (2004); SN/GRB neutrinos: S. Razzaque *et al.*, Phys. Rev. **D69** 023001 (2004)
[8] F. Mirabel, `arXiv:0805.2378v1` and references therein
[9] For LS5039: F. A. Aharonian *et al.*, J. Phys. Conf. Ser. **39** 408-415 (2006); see also S. Aiello *et al.*, Astropart. Phys. **28** 19 (2007)
[10] Th. Pradier, to be submitted to A&A
[11] R. H. Price, Phys. Rev. **D5** 2419 (1972); see also A. Nagar *et al.*, Phys. Rev. **D75** 044016 (2007)
[12] E. B. Segalis & A. Ori, Phys. Rev. **D64** 064018 (2001)
[13] C. Kouveliotou *et al.*, Astrophys.J.**510** L115-118 (1999); see also T. Terasawa *et al.*, Nature **434** 1110 (2005)
[14] K. Ioka *et al.*, Astrophys. J. **633**, 1013-1017 (2005); see also F. Halzen *et al.* `arXiv:astro-ph/0503348v1`
[15] J. A. de Freitas Pacheco, A&A **396**, 397-401 (1998)
[16] Th. Pradier *et al.*, Phys. Rev. **D63** 042002 (2001)
[17] N. Arnaud *et al.*, Phys. Rev. **D65** 042004 (2002)
[18] A. Heijboer, *Track reconstruction and point source searches with Antares*, Ph.D. dissertation, Universiteit van Amsterdam (2004) `http://antares.in2p3.fr/`
[19] S. D. Biller *et al.*, Phys. Rev. Lett. **83**, 2108-2111 (1999); see also J. Albert *et al.*, `arXiv:0708.2889v1`
[20] U. Katz, for KM3NET, these proceedings
[21] VIRGO Collaboration, Classical & Quantum Gravity **25** 114045 (2008)